EPJ manuscript No.
(will be inserted by the editor)

Polarised hydrogen line shapes in a magnetised plasma.

The Lyman α line

Note KW

Chantal Stehlé[1], Stéphane Brillant[2], and Gautier Mathys[2]

[1] DASGAL et UMR8633, Observatoire de Paris, 5 Place J. Janssen, F-92195 Meudon, France, e-mail: Chantal.Stehle@obspm.fr
[2] European Southern Observatory, Casilla 19001, Santiago 19, Chile

Received: date / Revised version: date

Abstract. The general profiles entering the polarised radiation transfer matrix for the hydrogen Lyα line in dense magnetised plasmas are studied. The Stark effect due to plasma electrons is treated by the Unified Theory. The contribution of fine structure is discussed. Ion dynamics effects are studied, by application of the Model Microfield Method (MMM). The validity of a simpler approach, based on the Simplified Unified Theory (SUT) is assessed, by comparison with the MMM.

PACS. 95.30 Astrophysical plasmas – 95.30.Dr Atomic processes and interactions – 32.70.Jz Line shapes, widths, and shifts

1 Introduction

The Zeeman splitting of the unpolarised Stark broadened lines of hydrogen [1–4], helium [5] and hydrogenic ions [6] is a well known tool for magnetic field diagnostics in stellar and laboratory plasmas. However the polarised spectrum of hydrogen in magnetised plasmas gives more information. The interpretation of observations of polarised hydrogen lines emerging from the atmospheres of magnetic stars requires an accurate treatment of the line broadening and an adequate description of the polarised transfer [7, 8]. Polarisation of the Stark broadened lines may be also used as a magnetic field diagnostic in Z pinch [3] and in Tokamak plasmas.

Mathys derived the formulation of the polarised absorption matrix, assuming cylindrical symmetry about the magnetic field [9,8]. He tabulated the intensity line shapes of Lyα, Lyβ, Hα for directions of observation parallel and perpendicular to the magnetic field [9,10].

Recently we revisited this formulation by including also the effects of the motional electric field, which is seen by the hydrogen atom moving with the velocity $\mathbf{v}$ in the magnetic field $\mathbf{B}$ [11]. This electric field ($\mathbf{F}_m = \mathbf{v} \times \mathbf{B}/c$), perpendicular to the magnetic field, breaks the cylindrical symmetry about the magnetic field. As suggested by Nguyen Hoe et al. [6], it introduces a coupling between the Doppler and Stark broadenings. To account for this, Brillant [12] proposed recently a new formulation of the generalised line shapes necessary to calculate the polarised transfer matrices. He applied it to the Hβ line. This formulation follows the approach of the Unified Theory [13], which describes the line shape in terms of frequency-dependent relaxation operators. These operators reflect the interaction between the radiating hydrogen atoms and the plasma charges (electrons and ions). Brillant's treatment includes simultaneously, for the first time, the effects of ion motions, of the magnetic field, and of the motional electric field. This approach is simplified, in the sense that the relaxation operators are calculated neglecting the effects of the magnetic and motional electric fields. As the main focus of interest was the line behaviours for large detunings $\Delta\lambda = \lambda - \lambda_0$ from the line centre λ_0, this approximation appears reasonable. It is one of the purposes of the present paper to check the validity of this approach, which will hereafter be called the "Simplified Unified Theory" (SUT).

This paper is devoted to the polarised hydrogen Lyα line. The magnetic field is supposed to be weak enough to be treated by the perturbation theory. The corresponding upper limit is approximately 5 MG for Lyα [14].

We shall assume that the nlm sublevels of hydrogen are equally populated for a given value of n, and we shall exclude the possibility of atomic coherences between these sublevels (fixed n). We shall also assume that the helicoidal motions of the plasma charges in the magnetic field introduce only negligible effects in the line shapes with respect to straight line paths. This is always the case for the ionic motions in standard plasmas. For the electrons, it requires the Debye screening length to be smaller than the gyration radius [1,5], or equivalently the electronic plasma frequency $\omega_{pe} = (4\pi e^2 N_e/m_e)^{1/2}$ to be larger than the Larmor angular frequency $\omega_L = eB/(2m_e c)$. Taking into account the numerical values of these two frequencies,

$$\omega_{pe} = 5.6\,10^4\, N_e^{1/2} \ \ (\mathrm{rd.s^{-1}}, \mathrm{cm^{-3}}),$$

Send offprint requests to: Chantal Stehlé

$$\omega_L = 8.8\,10^6\,B\ \ (\mathrm{rd.s}^{-1}, G)\,, \tag{1}$$

it can be seen that this condition may be not satisfied at low electronic densities N_e. This may have some effect in the line centers. But, in the line wings, the emission or absorption occurs when the perturbing charges are at shorter distances from the radiator than in the line center [15], and the radiative time of interest reduces from $|\omega_{pe}|^{-1}$ to $|\Delta\omega|^{-1}$, where $\Delta\omega$ is the detuning expressed in angular frequency units. Thus the previous condition must be replaced by the more general one:

$$\mathrm{Max}(\omega_{pe}, |\Delta\omega|) > \omega_L\,. \tag{2}$$

The first part of the paper is devoted to the presentation of the generalised absorption matrix which governs the transfer of polarised radiation. We shall also present the relation between the terms of the transfer matrix which are most directly related to the the unpolarised intensity and to the circular polarisation of the radiation (Stokes parameters I and V). Then, we shall review the relevant interaction potentials which modify the atomic structure of the radiating hydrogen atoms. In Sect. 3, we shall illustrate the effects of the magnetic field, fine structure, ion motion, and plasma density, both in the line centre and in the line wings. The effects of the motional electric field will be described in a subsequent paper.

2 Theory

In the presence of external fields ($\mathbf{B}$ and $\mathbf{F}_m$), the energy structure of the hydrogen atom is strongly modified and its spectrum is polarised. The radiative transfer is described by a vectorial equation for the Stokes vector $S = (I, Q, U, V)^t$ (see e.g. [16]).

2.1 Geometry

The radiation, of angular frequency ω, is propagating along the direction $\mathbf{e}_k$, which makes an angle θ with the magnetic field $\mathbf{B}$. The magnetic field is assumed to be parallel to the z-axis. Two mutually orthogonal polarisation unit vectors $\mathbf{e}_1$ and $\mathbf{e}_2$ are defined in the plane perpendicular to $\mathbf{e}_k$. The polarisation vector $\mathbf{e}_1$ is located in the plane defined by $\mathbf{B}$ and $\mathbf{e}_k$. The radiating hydrogen atom is moving with the velocity $\mathbf{v}$, which is decomposed in two components, perpendicular ($\mathbf{v}_\perp$) and parallel ($\mathbf{v}_\parallel$) to $\mathbf{B}$. We denote by ϕ the angle between the perpendicular component and the polarisation vector $\mathbf{e}_2$ (Figure 1). In this reference frame, the transfer along direction $\mathbf{e}_k$ of the Stokes vector is described in terms of 4×4 absorption and stimulated emission matrices, defined as [8]:

$$b_{abs(em)} = \begin{pmatrix} \eta_I & \eta_Q & \eta_U & \eta_V \\ \eta_Q & \eta_I & \rho_V & -\rho_U \\ \eta_U & -\rho_V & \eta_I & \rho_Q \\ \eta_V & \rho_U & -\rho_Q & \eta_I \end{pmatrix}. \tag{3}$$

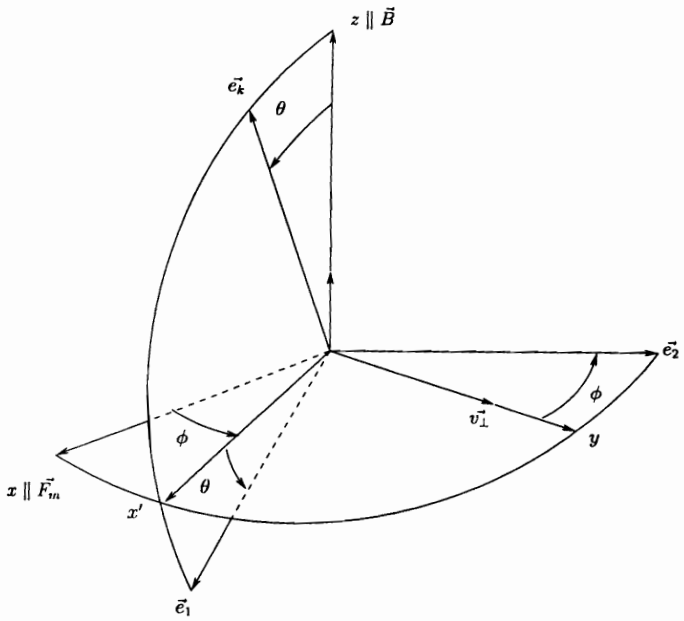

Fig. 1. Geometry of the system

This matrix can be split in two contributions [11]:

$$b(\omega, \mathbf{v}) = b_0(\omega, \mathbf{v}) + \cos 2\phi\, b_{cross}(\omega, \mathbf{v}). \tag{4}$$

The non-vanishing matrix elements of the first term, b_0, are given by

$$\begin{aligned} \eta_{I,0} &= (\cos^2\theta + 1)\,(I_{xx} + I_{yy})/2 + \sin^2\theta\, I_{zz}\,, \\ \eta_{Q,0} &= \sin^2\theta\,(I_{zz} - (I_{xx} + I_{yy})/2)\,, \\ \eta_{V,0} &= -\cos\theta\,(R_{xy} - R_{yx})\,, \\ \rho_{Q,0} &= \sin^2\theta\,(R_{zz} - (R_{xx} + R_{yy})/2)\,, \\ \rho_{V,0} &= \cos\theta\,(I_{xy} - I_{yx})\,. \end{aligned} \tag{5}$$

In the absence of a magnetic field, only $\eta_{I,0}$ differs from zero, and one has $\eta_{I,0} = 2I_{xx} = 2I_{yy} = 2I_{zz}$. The second contribution, proportional to $\cos 2\phi$, is due to the correlation between the Doppler shift and the motional electric field effects. This correlation term b_{cross} vanishes after average over the frequency, and disappears in the absence of a magnetic field. Its non-zero matrix elements are:

$$\begin{aligned} \eta_{I,cross} &= -\sin^2\theta\,(I_{xx} - I_{yy})/2\,, \\ \eta_{Q,cross} &= (\cos^2\theta + 1)\,(I_{xx} - I_{yy})/2\,, \\ \rho_{Q,cross} &= (\cos^2\theta + 1)\,(R_{xx} - R_{yy})/2\,. \end{aligned} \tag{6}$$

In Eqs. (5) and (6), I_{kl} (where k, l are any of x, y or z) is the real part, and R_{kl} the imaginary part, of the generalised line profile $\mathcal{I}_{kl}(\omega)$ defined by

$$\mathcal{I}_{kl}(\omega) = \sum_{a\alpha, b\beta} r_{aa} <a|D_k|\alpha><\beta|D_l|b> \ll a\alpha|\mathcal{T}(\omega)|b\beta\gg\,,$$

with

$$\begin{aligned} D_k &= \mathbf{e}_k \cdot \mathbf{D}\,, \\ D_l &= \mathbf{e}_l \cdot \mathbf{D}\,. \end{aligned} \tag{7}$$

D is the dipole operator of the hydrogen bound electron, r_{aa} is the statistical weight of state a, and $\mathcal{T}(\omega)$ is the Fourier transform at ω of the time evolution operator in the Liouville space $\mathcal{T}(t)$, averaged over all the interactions with the plasma charges.

Hereafter we denote by greek and roman letters the states corresponding to the lower (n) and upper (n') levels of the optical transition respectively. The calculation of the generalised line shapes is expressed in terms of a trace over the Liouville states. The trace is independent of the choice of the basis, for which we shall adopt the product of Hilbert basis vectors, defined by the quantum numbers n, l, m, m_s (n, principal quantum number; l and m, the orbital angular momentum and its projection along the quantification axis z; m_s, the projection of the spin). These states are thus the eigenstates of the hamiltonian H_0 (Equation 14), which neglects the fine structure effects. Thus the vector $|a\alpha \gg$ of the Liouville space stands for

$$|a\alpha \gg = |a >< \alpha| = |n_a l_a m_a m_{sa} >< n_\alpha l_\alpha m_\alpha m_{s\alpha}| \quad (8)$$

(for the Lyα line, $n_a = 2$ and $n_\alpha = 1$). The matrix elements of the Liouville time evolution operator $\mathcal{T}(t)$ are defined in terms of the Hilbert time evolution operator $T(t)$ by

$$\ll a\alpha|\mathcal{T}(t)|b\beta \gg = < a|T(t)|b > \times < \alpha|T(t)|\beta >^* \ . \quad (9)$$

This Liouville operator $\mathcal{T}(t)$ satisfies the equation of evolution:

$$i\hbar \frac{d\mathcal{T}(t)}{dt} = L\,\mathcal{T}(t) \ \text{ with } \mathcal{T}(0) = 1\,, \quad (10)$$

where the Liouville operator L is connected to the Hilbert hamiltonian H by

$$\ll a\alpha|L|b\beta \gg = \delta_{\alpha,\beta} < a|H|b > - \delta_{a,b} < \alpha|H|\beta > \ . \quad (11)$$

As the initial magnetic sublevels a are equally populated, it is possible to move the terms $r_{aa} = r_0$ out of the trace in Equation (7). This allows us to normalize in the following the line profiles $\mathcal{I}(\omega)$ to

$$r_0 \sum_{a\alpha,k} | < a|D_k|\alpha > |^2 = r_0 \sum_{a\alpha} S_{a\alpha}, \quad (12)$$

where $S_{a\alpha}$ is the usual line strength. As a consequence, $\eta_{I,0}$ is normalised to 2/3.

2.2 The hydrogen atom in the magnetic field

The evolution operator in the Hilbert space of the moving hydrogen atom in the absence of interactions with surrounding charges is described by the equation

$$i\hbar \frac{dT(t)}{dt} = H\,T(t) \ \text{ with } T(0) = 1\,, \quad (13)$$

where the hamiltonian H is the sum of the hamiltonian of the free atom (without magnetic field or fine structure effects), H_0, and of the hamiltonians due to the fine structure coupling H_{fs}, to the Zeeman interaction with the magnetic field H_{Zeem}, and to the dipolar interaction with the motional electric field H_{mot}. In the considered geometry, one has:

$$H = H_0 + H_{fs} + H_{Zeem} + H_{mot}\,, \quad (14)$$

where

$$H_{Zeem} = \hbar\omega_L(L_z + 2S_z)\,,$$
$$H_{mot} = -eD_x v_\perp B/c\,. \quad (15)$$

The corresponding Liouville operators will be denoted by L, L_0, L_{fs}, L_{Zeem} and L_{mot}. The fine structure hamiltonian includes the relativistic correction to the energy, the spin-orbit and the Darwin terms [17]. Lamb shift contribution is not considered here.

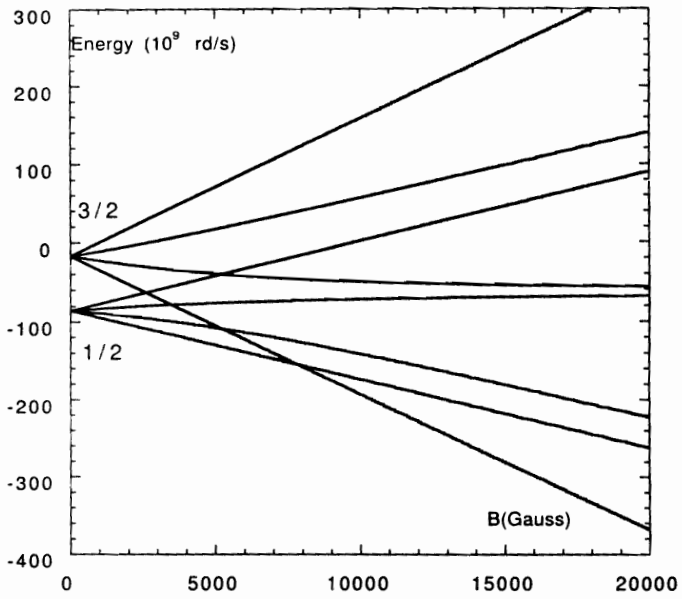

Fig. 2. Variations of the eigenenergies of the hamiltonian H (Equation 14), in units of 10^9 rd/s, for the level $n = 2$ of hydrogen in a magnetic field B (in G) and without motional electric field effect. The values of the quantum number J (1/2 and 3/2) associated to the eigenstates at low magnetic field values are reported along the ordinate axis.

At large values of the magnetic field, one may neglect altogether the effects of fine structure coupling, and of the motional electric field. Thus the eigenenergies are linear in B. They are $\pm 2\hbar\omega_L B$, $\pm\hbar\omega_L B$ and 0 for $n = 2$. The pattern of the Lyα line is then a regular Zeeman triplet. At low magnetic field values, the fine structure effects are significant (case of the anomalous Zeeman effect), and the line splits into four lines for the $2p_{1/2} - 1s_{1/2}$ and 6 lines for the $2p_{3/2} - 1s_{1/2}$ transitions [17]. These first two cases, low field ($B < 5\,10^3$ G), and large field regimes ($5\,10^3 < B < 5\,10^4$ G), are illustrated for the level $n = 2$ in Figure 2. The structure of atomic hydrogen in this range of magnetic field values is well known. The situation is more complex if one introduces the effects of an additive electric

field [18], which is, in the present case, the motional field perpendicular to the magnetic field . Eigenstates of hydrogen in crossed fields B_z, F_x are analytical, if one omits the contributions of the fine structure and of the quadratic Zeeman term [1,19]. For example the four eigenenergy deviations from the unperturbed energy value of the $n = 2$ level are given by

$$E(B_z, F_x) = \pm\hbar\omega_L \left(1 + \left(\frac{3ea_0F_x}{\hbar\omega_L}\right)^2\right)^{1/2}, \; 0, \; 0 \quad (16)$$

and reduce obviously to $\pm\hbar\omega_L$ and 0 in the absence of motional Stark effect ($F_x = 0$). For a perpendicular velocity $v_\perp$ equal to the thermal velocity of the hydrogen atoms ($(2kT/m_H)^{1/2}$), the typical energy splitting due to motional Stark effect is $\hbar\,\omega_x$, with:

$$\omega_x = ea_0F_x/\hbar = 1032\; B\,T^{1/2} \;\; (\mathrm{rd.s^{-1}}, \mathrm{G}, \mathrm{K}). \quad (17)$$

The comparison between ω_x and ω_L indicate that, for temperatures of the order of 10000K, the effects of the motional electric field can be treated within the perturbation theory, leading to an energy correction quadratic in the magnetic field [11].

2.3 Plasma broadening

Let us now discuss the effects of the interactions between the hydrogen atom and the surrounding plasma charges. This plasma Stark effect may be described by the leading dipolar interaction of the hydrogen atom with the ionic and electronic microfields $\mathbf{F}_i$ and $\mathbf{F}_e$. The corresponding interaction potential is, in the Hilbert space,

$$V = -\mathbf{D}\cdot(\mathbf{F}_i + \mathbf{F}_e). \quad (18)$$

The electronic and ionic microfields are random vectors, described by field distribution functions [20,21]. Due to their different time scales, the two random plasma fields play a different rôle in the line broadening. The electronic contribution can be described in terms of collisions, whereas the ionic contribution varies between the collisional limit at low densities and the static limit at large densities.

The line shape computation requires one to estimate the Liouville evolution operator $\langle\mathcal{T}(t)\rangle_{e,i}$ or its Fourier transform $\langle\mathcal{T}(\omega)\rangle_{e,i}$, averaged over the plasma states (i.e., initial positions and velocities of all the free charges, electrons and ions). In this paper, we describe the electronic and ionic Stark broadenings by the Model Microfield Method (MMM) [22–25], which is presently the only method appropriate to cover the different regimes at low and high densities, and to ensure also the convergence towards the static limit in the line wings.

Let us, for a while, suppose that the ionic contribution to the broadening can be described within the static approximation. This means in particular that, for each fixed value of the ionic microfield $\mathbf{F}_i$, with the probability $P(\mathbf{F}_i)$, the evolution operator can be averaged over all the interactions with the electrons, and expressed, as suggested by the Relaxation [13] and Unified Theories [26], in terms of the frequency dependent electronic relaxation operator $\gamma_e(\omega)$, by:

$$\langle\mathcal{T}(\mathbf{F}_i)\rangle_e = \frac{i}{\pi}[\omega I - L/\hbar - \mathbf{D}\cdot\mathbf{F}_i/\hbar + \mathrm{i}\gamma_e(\omega)]^{-1}. \quad (19)$$

In general, one can neglect the dependence of the relaxation operator $\gamma_e(\omega)$ on the ionic microfield value. Taking as a reference Stark splitting the splitting due to the normal electric field value, $F_0 = 2.603\,e\,N_e^{2/3}$, and as a typical time of interest the inverse of the plasma frequency, this last simplification requires in the case of the Lyα line, that the electronic plasma frequency ω_{pe} be larger than the frequency corresponding to the typical Stark energy splitting $3e\,a_0\,F_0/\hbar = 9\,N_e^{2/3}$ (rd/s, cm^{-3}), or:

$$N_e < 5.10^{22}\ \mathrm{cm^{-3}}. \quad (20)$$

This approximation is always satisfied under typical plasma conditions.

We shall also assume that the fine structure effects (with a typical frequency splitting of $7\;10^{10}$ rd/s) and the Zeeman splitting (and the Stark motional effect) have no contribution in the calculation of the electronic relaxation operator, which means, in the same way, that $\omega_{pe} > \omega_L$ and $\omega_{pe} > \omega_{fs}$, or respectively

$$N_e > 2.5\,10^4\,B^2 \;\; (\mathrm{cm^{-3}}, \mathrm{G}),$$
$$N_e > 1.5\,10^{12} \;\; (\mathrm{cm^{-3}}). \quad (21)$$

The electronic broadening can be obtained very simply, in the following manner: we calculate the evolution operator, $\langle\mathcal{T}(\omega)\rangle_e$, for a plasma containing free electrons, moving in a uniform background of positive charges, neglecting the effects of the magnetic field, and of the fine structure. Then, from an expression similar to Equation (19), with $L = L_0$, and $F_i = 0$, one deduces the frequency dependent electronic relaxation operator $\gamma_e(\omega)$. This electronic evolution operator $\langle\mathcal{T}(\omega)\rangle_e$ is calculated by MMM, as in previous unpolarised line shapes calculations [24,25,27], using the MMM relation

$$\begin{aligned}\langle\mathcal{T}(\omega)\rangle_e &= \langle\mathcal{T}_s(\mathbf{F}_e, z_e)\rangle_e + \langle\nu_e\mathcal{T}_s(\mathbf{F}_e, z_e)\rangle_e \\ &\quad\times\langle\nu_e I - \nu_e^2\mathcal{T}_s(\mathbf{F}_e, z_e)\rangle_e^{-1}\langle\nu_e\mathcal{T}_s(\mathbf{F}_e, z_e)\rangle_e, \\ &= \frac{i}{\pi}[\omega I - L_0/\hbar + i\gamma_e(\omega)]^{-1}, \end{aligned} \quad (22)$$

where $\nu_e = \nu(F_e)$ and $\mathcal{T}_s(z_e)$ is the Laplace transform, at $z_e = \omega + i\nu_e$, of the evolution operator calculated for a static electronic field. The angle brackets denote averages over the electronic field distribution function, such as, for example:

$$\langle\mathcal{T}_s(\mathbf{F}_e, z_e)\rangle_e = \int_0^\infty \mathcal{T}_s(\mathbf{F}_e, \omega + i\nu_e)\,P(F_e)\,dF_e. \quad (23)$$

The frequency jump ν_e allows one to take into account the dynamical properties of the electronic microfield. One has

$$\mathcal{T}_s(\mathbf{F}_e, z_e) = \frac{i}{\pi}\,[z_e\,I - L/\hbar - \mathcal{D}\cdot\mathbf{F}_e/\hbar]^{-1}. \quad (24)$$

To obtain the plasma averaged evolution operator, one needs now to carry out the average over the realisations of the ionic microfield. This ionic contribution is also obtained using the MMM formalism. Thus, the ion averaged evolution operator $\langle \mathcal{T}(\omega)\rangle_i$ is obtained by an expression similar to Equation (22), replacing the electronic field distribution function and frequency jump by the ionic ones, i.e.:

$$\begin{aligned}\langle \mathcal{T}(\omega)\rangle_i &= \langle \mathcal{T}_s(\mathbf{F}_i, z_i)\rangle_i + \langle \nu_i \mathcal{T}_s(\mathbf{F}_i, z_i)\rangle_i \\ &\times \langle \nu_i I - \nu_i^2 \mathcal{T}_s(\mathbf{F}_i, z_i)\rangle_i^{-1} \langle \nu_i \mathcal{T}_s(\mathbf{F}_i, z_i)\rangle_i \,. \quad (25)\end{aligned}$$

In this expression, $\nu_i = \nu(F_i)$ and the static evolution operator $\mathcal{T}_s(\mathbf{F}_i, z_i)$, averaged over the electron contributions, is given by

$$\mathcal{T}_s(\mathbf{F}_i, z_i) = \frac{i}{\pi}[(\omega + i\,\nu_i)\, I - L/\hbar - \mathcal{D}\cdot\mathbf{F}_i/\hbar + i\,\gamma_e(\omega)]^{-1}\,, \quad (26)$$

where $\mathcal{D}$ is the Liouville operator associated to the dipole Hilbert operator $\mathbf{D}$.

The *total* frequency dependent relaxation rate $\gamma(\omega)$ may be deduced from the evolution operator averaged over the interactions with the plasma *electrons and ions* by the following expression

$$\langle \mathcal{T}(\omega)\rangle_{e,i} = \frac{i}{\pi}\,[\omega I - L/\hbar - + i\,\gamma(\omega)]^{-1}\,. \quad (27)$$

2.4 Large detunings

Let us in this section neglect the effects of the motional electric field and suppose that the light propagation is parallel to the magnetic field (i.e., $\theta = 0$ in Equations (5) and (6)).

We shall focus our attention on the two terms η_I and η_V of the absorption matrix. Introducing the irreducible representation D_q ($q = 0, \pm 1$) of the dipole vector operator $\mathbf{D}$, one has:

$$\begin{aligned}\eta_I(\omega) &= \mathrm{Tr}(D_1 D_{-1} + D_{-1} D_1)\,\mathrm{Im}\mathcal{T}(\omega)\,, \\ \eta_V(\omega) &= \mathrm{Tr}(D_1 D_{-1} - D_{-1} D_1)\,\mathrm{Im}\mathcal{T}(\omega)\,. \quad (28)\end{aligned}$$

In the absence of plasma effects, the broadening is only due to spontaneous radiative decay. Neglecting also the fine structure, the radiative broadening γ_r is negligible for the $2s$ state (metastable state) and $\gamma_{1s2p,1s2p;r} = 0.5 A_{2p,1s}$ for each $2pm$ state ($A_{2p,1s} = 6.265\ 10^8\ \mathrm{s}^{-1}$, [28]).

In this case, the intensity profile is a sum of two lorentzians, one peaked at $-\omega_L$ and the second at ω_L, whereas η_V is the difference between these two lines, which do not interfere (because they correspond to mutually orthogonal polarisations). One obtains:

$$\eta_I(\omega) = \frac{1}{3\pi}\left(\frac{\gamma_{1s2p,1s2p;r}}{(\Delta\omega - \omega_L)^2 + \gamma^2_{1s2p,1s2p;r}} + \frac{\gamma_{1s2p,1s2p;r}}{(\Delta\omega + \omega_L)^2 + \gamma^2_{1s2p,1s2p;r}}\right),$$

$$\eta_V(\omega) = \frac{1}{3\pi}\left(\frac{\gamma_{1s2p,1s2p;r}}{(\Delta\omega - \omega_L)^2 + \gamma^2_{1s2p,1s2p;r}} - \frac{\gamma_{1s2p,1s2p;r}}{(\Delta\omega + \omega_L)^2 + \gamma^2_{1s2p,1s2p;r}}\right). \quad (29)$$

In the line wings, the effect of the Zeeman splitting is negligible for η_I. Thus one has, for any value of θ:

$$\begin{aligned}\eta_I(\omega) &= \frac{2}{3}\frac{\gamma_{1s2p,1s2p;r}}{\pi\Delta\omega^2}\,, \\ \eta_V(\omega) &= \frac{4}{3}\frac{\omega_L\cos\theta\,\gamma_{1s2p,1s2p;r}}{\pi\Delta\omega^3} = \omega_L\cos\theta\frac{d\eta_I}{d\omega}\,. \quad (30)\end{aligned}$$

The latter equation is often used in the interpretation of astrophysical observations to determine the projection of the magnetic field along the line of sight ($B\cos\theta$) (e.g. [29]). It assumes (although this is seldom explicitly stated) that the coupling with the surroundings, which leads to line broadening, preserves the state quantification along the z axis imposed by the magnetic field. However, this is not the case in a plasma. Hence, Stark broadening mixes together states with different m_l (or m_j) quantum numbers.

This "mixing" is larger at high densities and in the line wings, where the interaction between the radiating hydrogen atom and the plasma gives the dominant contribution to $\eta_I(\omega)$. In the line wings, the "static" limit for both the electrons and the ions is reached, and one recovers the usual static limit for η_I . One has, for a detuning $\Delta\omega$ from line center, and for the Lyα line:

$$\eta_I(\omega) = \frac{2}{3}\frac{C_{Ly\alpha}}{|\Delta\omega|^{5/2}}\,. \quad (31)$$

Note that the intensity in the line wings is reduced by a factor 2/3 with respect to the Holtsmark wing intensity of the standard case. The latter is normalised to unity, whereas, as seen from Equation (28), η_I is here normalised to 2/3 and η_V to 0 . The numerical value of the constant $C_{\mathrm{Ly}\alpha}$ is equal, for $\Delta\omega$ expressed in rd.s^{-1}, and the Stokes component η_I in s.rd^{-1}, to

$$C_{\mathrm{Ly}\alpha} = 13.5\, N_e \quad (32)$$

(where the electronic density N_e is in cm^{-3}). This Holtsmark line wing limit gives for the total relaxation operator (including the contributions of the electrons and the ions):

$$\gamma_{1s2p,1s2p}(\omega) = \pi\, C_{\mathrm{Ly}\alpha}|\Delta\omega|^{-1/2}. \quad (33)$$

One obtains, in the line wings, whatever the form of $\gamma(\omega)$:

$$\begin{aligned}\eta_I(\omega) &= \frac{2}{3\pi}\frac{\gamma_{1s2p,1s2p}(\omega)}{\Delta\omega^2}\,, \\ \eta_V(\omega) &= \frac{4}{3\pi}\frac{\gamma_{1s2p,1s2p}(\omega)}{\Delta\omega^3}\,, \quad (34)\end{aligned}$$

which gives the more general relation, valid for all the lines and each value of θ

$$\eta_V(\omega) = 2\omega_L\cos\theta\frac{\eta_I(\omega)}{\Delta\omega}\,. \quad (35)$$

This relation coincides with the previous ones, in the case where the relaxation operator does not depend on the frequency (which is the case for pure radiative broadening). Deviations from the previous rule reflect the fact that atomic structure modifications due to short-range potentials may dominate the line wing intensity.

2.5 Simplified Unified Theory

It has been shown that the line shape can be expressed in terms of a relaxation operator $\gamma(\omega)$ (Equation (27)). This operator is composed from two additive contributions, one from the plasma electrons, $\gamma_e(\omega)$, and one from the ions, $\gamma_i(\omega)$. Strictly speaking, these two operators must be calculated with the full hamiltonian H (Equation (14)). We already showed that the electronic relaxation operator is independent of the external field and of the fine structure. This is also the case for the ionic relaxation operator at low densities when $\omega_{pi} > \omega_L$ and $\omega_{pi} > \omega_{fs}$, where ω_{pi} is the ionic plasma frequency defined for a plasma of protons as $\omega_{pi} = \omega_{pe}(2\,m_e/m_H)^{1/2}$, and ω_{fs} is the typical fine structure frequency splitting (about $7\,10^{10}$ rd s^{-1}). This corresponds to the following conditions:

$$N_e > 2\,10^7\,B^2 \text{ and } N_e > 10^{15} \ (\text{cm}^{-3}, \text{G}) . \qquad (36)$$

Obviously, the first condition may be not satisfied for low density plasmas ($N_e < 10^{15}\text{cm}^{-3}$) and magnetic field values of the order of 10^4 G. Nevertheless, as mentioned before for the electronic broadening, it is justified to neglect the effect of the magnetic field in the calculation of the total relaxation rates, far from the Zeeman resonances, because the time of interest reduces from ω_L^{-1} to $|\Delta\omega|^{-1}$.

Thus, in SUT, the total relaxation operator, denoted by $\gamma_{SUT}(\omega)$, is deduced from Equation (27) where magnetic field and fine structure effects are neglected (i.e., taking only $L = L_0$ in Equations (22-27)). The line shape, which includes the magnetic field effects, is given by Equation (7), where $\mathcal{T}_{SUT}(\omega)$ is expressed in terms of $\gamma_{SUT}(\omega)$ by

$$\mathcal{T}_{SUT}(\omega) = i\,\pi\,[\omega I - L/\hbar - + i\,\gamma_{SUT}(\omega)]^{-1} . \qquad (37)$$

In this expression, L contains the contributions of the magnetic field. It may include or not the fine structure contribution. As to the relaxation operator $\gamma_{SUT}(\omega)$, it is calculated without the latter effects (i.e., taking only $L = L_0$).

3 Numerical results

3.1 Numerical method

As indicated previously, the electronic relaxation operator is first calculated, in the frame of the Model Microfield Method, neglecting the effects of the magnetic field, the motional electric effect, and the fine structure. Only the real part of this operator is numerically accurate for all values of the detuning. In the line wings it converges towards the usual static limit in $|\Delta\omega|^{-1/2}$. As may be seen from expression (22), the imaginary part of $\gamma_e(\omega)$ cannot be obtained from the inversion of $\langle\mathcal{T}(\omega)\rangle_e$, because the value $\langle\mathcal{T}(\omega)\rangle_e^{-1}$ is dominated , at large detunings, by $\Delta\omega$. To overcome this difficulty, the imaginary part of $\gamma_e(\omega)$ is numerically obtained from the real part, by using the Kramers-Kronig relation [30]. It is possible to prove that the imaginary and real parts are identical in the line wings Holtsmark limit [12].

Knowing $\gamma_e(\omega)$, it is possible to calculate the full profiles, including (or not) the effects of the fine structure, the magnetic field and the electric motional field. This step is performed using the Model Microfield Method. Effects of ionic motions are also tested against a static ion computation. The latter is obtained setting $\nu(F_i)$ equal to zero in Equation (25). The integration over the realizations of the ionic microfield in the presence of a magnetic field is more difficult than in the usual case of non-magnetic plasmas. Beside the standard integration over the electric microfield modulus, an angular integration over the directions of the microfield vector is necessary. These directions are characterized by two angles, θ_F and ϕ_F, which are respectively the angle between **F** and the magnetic field (chosen along the z axis) and the angle between the plane defined by **B** and **F** and the xz plane. In the absence of motional electric field (parallel to the x axis), one avoids the integration over the azimuth angle ϕ_F using the properties of the rotation matrices. In this case, the average over ϕ_F leads to the cancellation of the matrix elements of $\mathcal{T}(\omega)$ between the states $|n_a l_a m_a m_{sa}; n_\alpha l_\alpha m_\alpha m_{s\alpha} \gg$ and $|n_b l_b l_b m_{sb}; n_\beta l_\beta m_\beta m_{s\beta} \gg$ such that:

$$m_a + m_{sa} - m_\alpha - m_{s\alpha} = m_b + m_{sb} - m_\beta - m_{s\beta} . \qquad (38)$$

If the effect of the motional electric field was included, the numerical integration over ϕ_F should be performed numerically. Hence this effect breaks the cylindrical symmetry around the z axis. Field distribution functions are taken from Hooper [20,21]. The frequency jump is defined by the usual expressions given by Brissaud et al. [31]. We shall illustrate for three different electronic densities, equal to 10^{13}, 10^{15} and 10^{17} cm^{-3} ($\omega_{pe} = 1.8\,10^{11}$, $1.8\,10^{12}$, $1.8\,10^{13}$ rd.s^{-1}), and magnetic field strengths equal to 10^3, $5\,10^3$, and $2\,10^4$ G ($\omega_L = 8.810^9$, $4.4\,10^{10}$, $1.76\,10^{11}$ rd.s^{-1}), the fine structure effects (with an order of magnitude for the splitting of $\omega_{fs} = 7.\,10^{10}$ rd.s^{-1}) and the correlation between the absorption matrix elements η_I and η_V. The temperature is chosen equal to 10^4 K. The angle θ between the radiation propagation vector and the magnetic field is set to 0 (observation parallel to the magnetic field).

The detuning is given in 10^9 rd.s^{-1}. As a consequence, the area normalised intensity is given in 10^{-9} s.rd^{-1}. Using this choice of units, the η_I Holtsmark wing intensity is $2.85\,10^{-13}N_e/|\Delta\omega|^{5/2}$. Note again that η_I is area normalised to 2/3.

The correspondence between the detuning expressed in units of 10^9 rd.s^{-1} and expressed in Angströms is given by

$$\Delta\lambda(\text{Å}) = 7.84\ 10^{-5}(\Delta\omega/(10^9\text{rd.s}^{-1})). \qquad (39)$$

The contributions to broadening of spontaneous emission decay and of Doppler effect are not included here, because we are mainly interested in analyzing the intrinsic variations of the line, with a view to predicting systematic behaviours for all the lines of hydrogen and hydrogenic ions. Its inclusion can be easily performed by standard convolution with the pure Doppler line shape (whose halfwidth is equal to 5.55 10^2 ($\times$ 10^9 rd.s^{-1})).

3.2 Fine structure effects

We calculated the line shapes for the three electronic densities. Figures 3, 4, 5, 6 illustrate for the intensity profile η_I the fine structure effects in the line center for the three considered magnetic fields values. The variations of the profile η_V are shown in Figures 7, 8, and 9. Ion dynamics effects are included, but Doppler broadening is not.

At 10^{17} cm^{-3} (Figures 3, 7), the Zeeman pattern is not resolved and the fine structure effects are negligible. This is due to the dominant effect of Stark broadening. The Stark halfwidth is of the order of 700 (10^9 rd.s^{-1}) whereas ω_L varies between 8.8 at 10^3 G and 176 at 2 10^4 G, and ω_{fs} is about 70.

At the intermediate density, 10^{15} cm^{-3} (Figures 4, 8), the pure Stark broadening has a halfwidth of about 50. The Zeeman pattern is resolved at 2 10^4 G, but this is not the case for the two smaller values of the magnetic field. The fine structure introduces a small asymmetry in the line shapes.

At the lowest density, 10^{13} cm^{-3} (Figures 5, 6, 9), the fine structure splitting is completely resolved. The combined effects of the magnetic field and fine structure lead to a very complicated pattern. These conclusions are valid for both profiles η_I and η_V.

Let us now discuss the effect of fine structure in the line wings. Towards large detunings, the line shape is sensitive to short range interactions, leading to large values of the interaction potential due to the electric field. The intensity is dominated by electric field effects, leading to an Holtsmark wing intensity in $|\Delta\omega|^{-5/2}$ for η_I and to a variation of η_V due to the effects of both the polarising magnetic field and the electric interaction. As a consequence, one expects a negligible contribution of the fine structure for both η_I and η_V. This point is verified in Figures 10, 11 and 12 for η_I, and in Figure 13 for η_V .

3.3 Ion dynamics effects

In order to test the effects of ion dynamics on the line shapes, we performed the computation of the profiles in the static ion approximation (i.e., $\nu(F_i) = 0$ in Equation (25)), and compared the MMM profiles with the static ones. Ion dynamics effects are very large in the line centers, as shown in Figures 14, 15, 16. They are enhanced by fine structure effects and are more spectacular towards low densities. At the highest density, the profiles obtained neglecting fine structure effects have not been represented here, because they are indistinguishable from those shown in Figure 14 on the scale used.

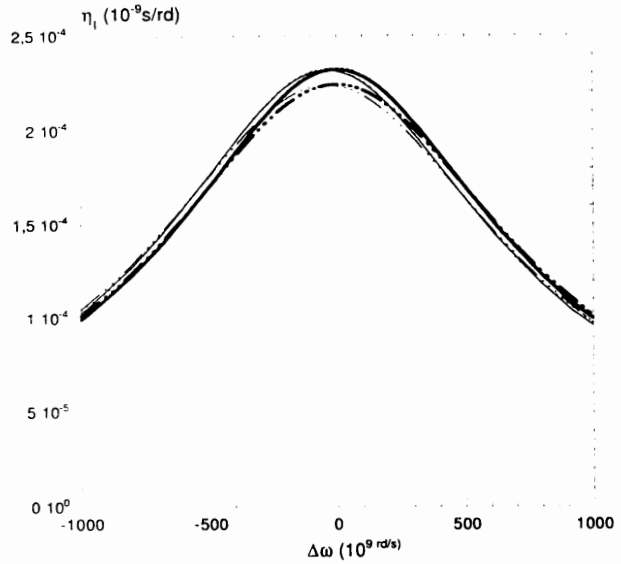

Fig. 3. Fine structure effects on η_I in the center of the Lyα line at an electronic density of 10^{17} cm^{-3}, for three values of the magnetic field: 10^3 (dotted line), 5 10^3 (solid line), and 2 10^4 G (dots-dashes). The profiles including the fine structure effects are represented as thin lines, those neglecting the fine structure effect as thick lines. Ion dynamics effects are included.

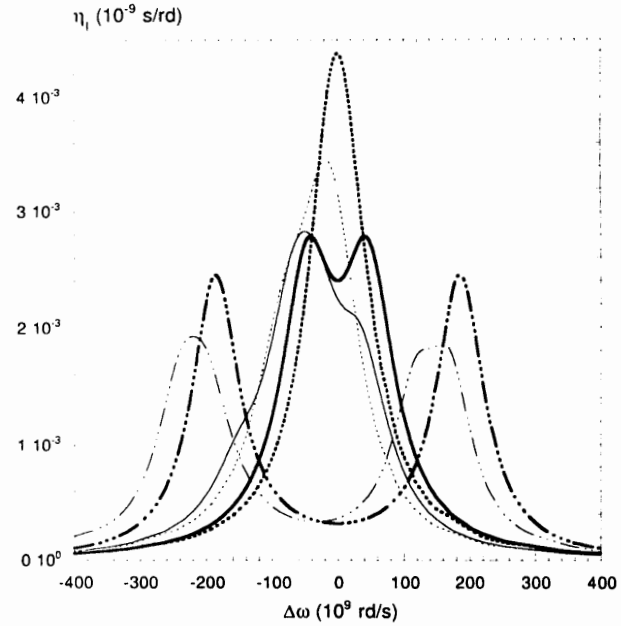

Fig. 4. Same as Figure 3 but for an electronic density of 10^{15} cm^{-3}.

3.4 Validity of the SUT

The description of the line shape by the Simplified Unified Theory uses a frequency-dependent relaxation operator $\gamma(\omega)$, to include the ion and electron contributions in the Stark broadening. This operator is obtained within the MMM theory, hence it includes electron and ion dy-

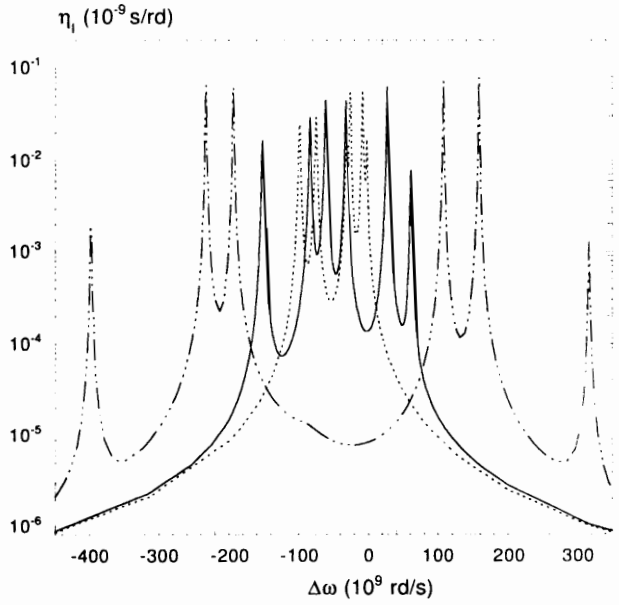

Fig. 5. Fine structure effects on η_I in the center of the Lyα line at an electronic density of 10^{13} cm^{-3}, for three values of the magnetic field: 10^3 (dotted lines), 5 10^3 (solid lines), and 2 10^4 G (dots-dashes). Only the profiles including the fine structure effects are represented (compare to Fig. 6). Ion dynamics effects are included.

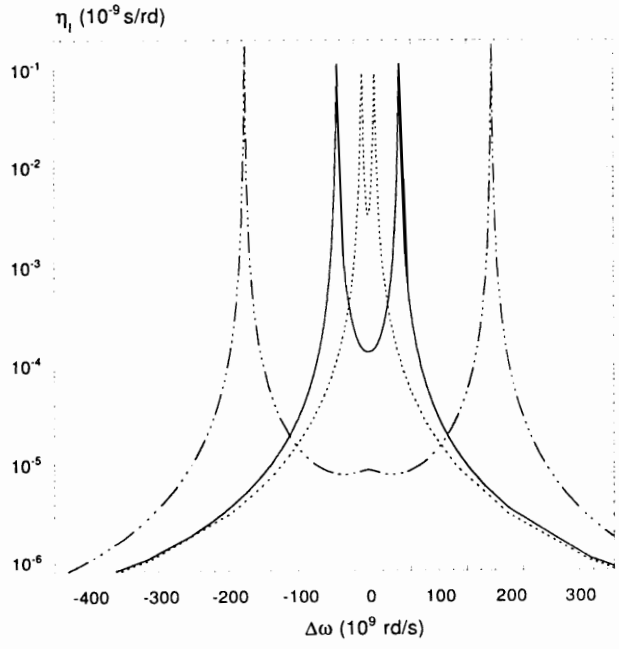

Fig. 6. Same as Figure 5, but without fine structure effects (compare to Fig. 5).

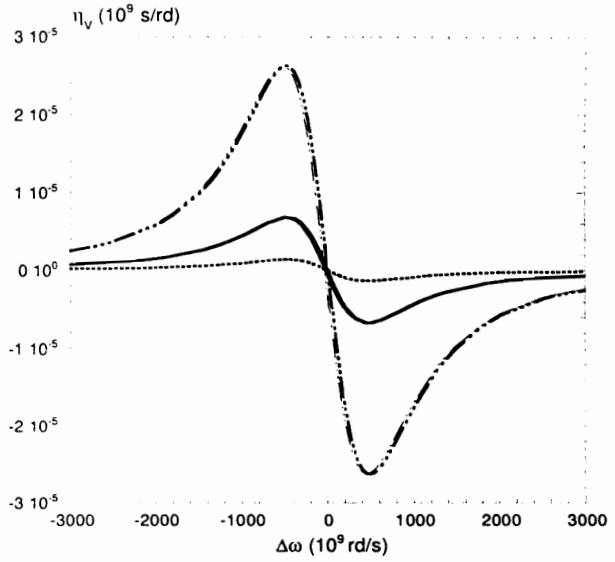

Fig. 7. Fine structure effects on η_V in the center of the Lyα line at an electronic density of 10^{17} cm^{-3}, for three values of the magnetic field: 10^3 (dotted lines), 5 10^3 (solid lines), and 2 10^4 G (dots-dashes). The profiles including the fine structure effects are represented as thin lines, those neglecting the fine structure effect as thick lines. Ion dynamics effects are included.

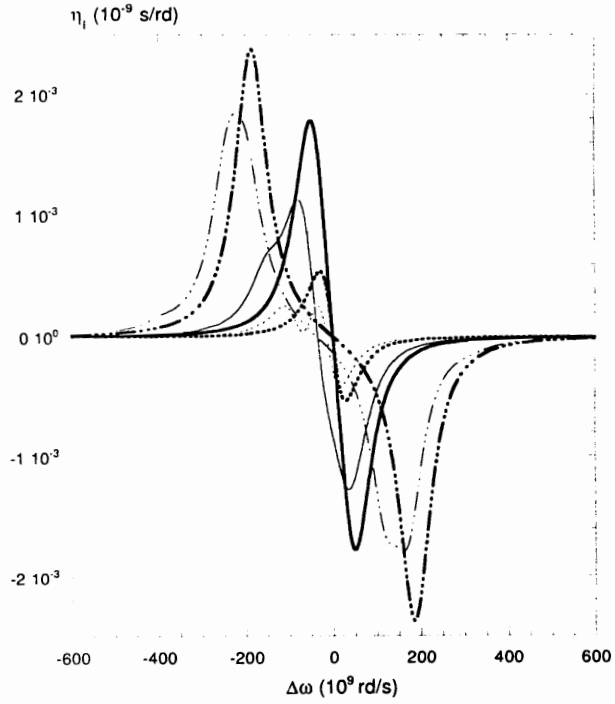

Fig. 8. Same as Figure 7 but for an electronic density of 10^{15} cm^{-3}.

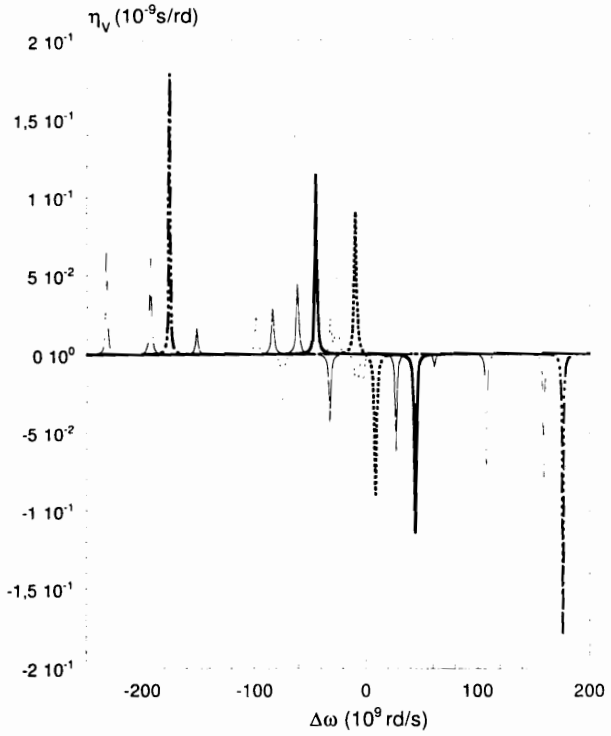

Fig. 9. Same as Figure 7 but for an electronic density of 10^{13} cm^{-3}.

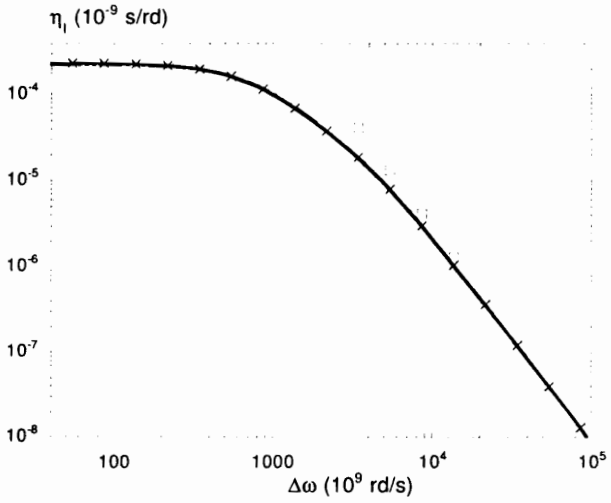

Fig. 10. Fine structure effects on η_I in the wing of the Lyα line (large positive detuning) at an electronic density of 10^{17} cm^{-3}, without magnetic field (crosses), and for three values of the magnetic field: 10^3, 5 10^3, and 2 10^4 G. All profiles are indistinguishable on this scale. The asymptotic Holtsmark wing is represented with squares.

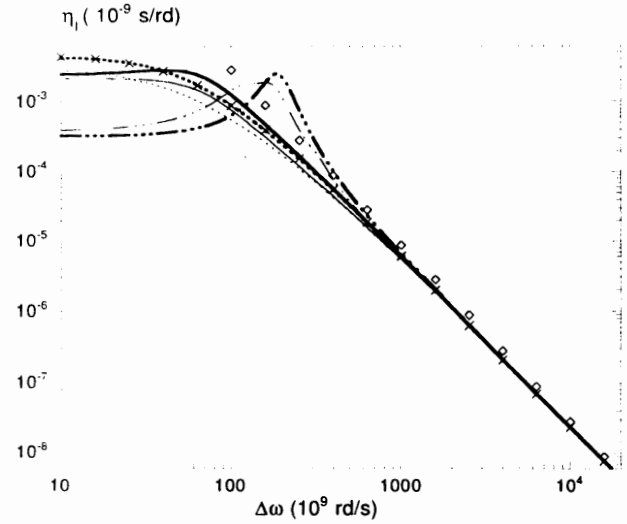

Fig. 11. Fine structure effects on η_I in the wing of the Lyα line (large positive detuning) at an electronic density of 10^{15} cm^{-3}, for three values of the magnetic field: 10^3 (dotted lines), 5 10^3 (solid lines), and 2 10^4 G (dots-dashes). The profiles including the fine structure effects are represented as thin lines, those neglecting the fine structure effect as thick lines. The crosses correspond to the case $B = 0$, without fine structure. The asymptotic Holtsmark wing is represented with diamonds.

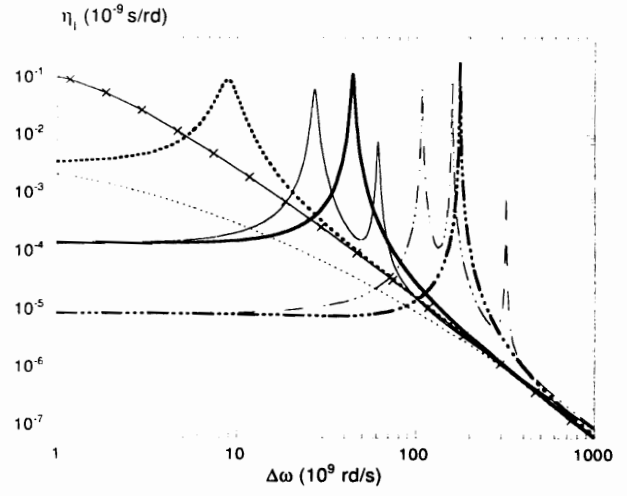

Fig. 12. Fine structure effects on η_I in the wing of the Lyα line (large positive detuning) at an electronic density of 10^{13} cm^{-3}, for three values of the magnetic field: 10^3 (dotted lines), 5 10^3 (solid lines), and 2 10^4 G (dots-dashes). The profiles including the fine structure effects are represented as thin lines, those neglecting the fine structure effect as thick lines. The crosses correspond to the case $B = 0$, without fine structure.

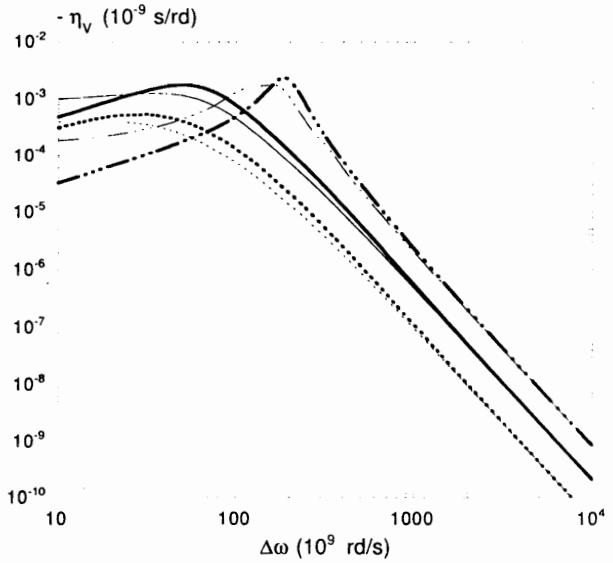

Fig. 13. Fine structure effects on η_V in the wing of the Lyα line (large positive detuning) at an electronic density of 10^{15} cm^{-3}, for three values of the magnetic field: 10^3 (dotted lines), 5 10^3 (solid lines), and 2 10^4 G (dots-dashes). The profiles including the fine structure effects are represented as thin lines, those neglecting the fine structure effect as thick lines.

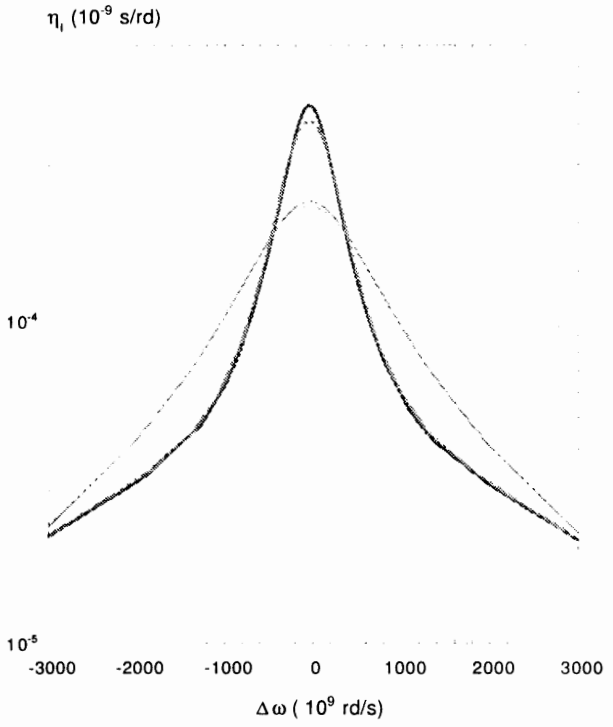

Fig. 14. Ion dynamics effects on η_I for the Lyα line at an electronic density of 10^{17} cm^{-3}, for three values of the magnetic field: 10^3 (dotted lines), 5 10^3 (solid lines), and 2 10^4 G (dots-dashes). Thick lines correspond to profiles computed with the static approximation for the ions, thin lines to profiles taking ion dynamics into account. Fine structure effects are also included.

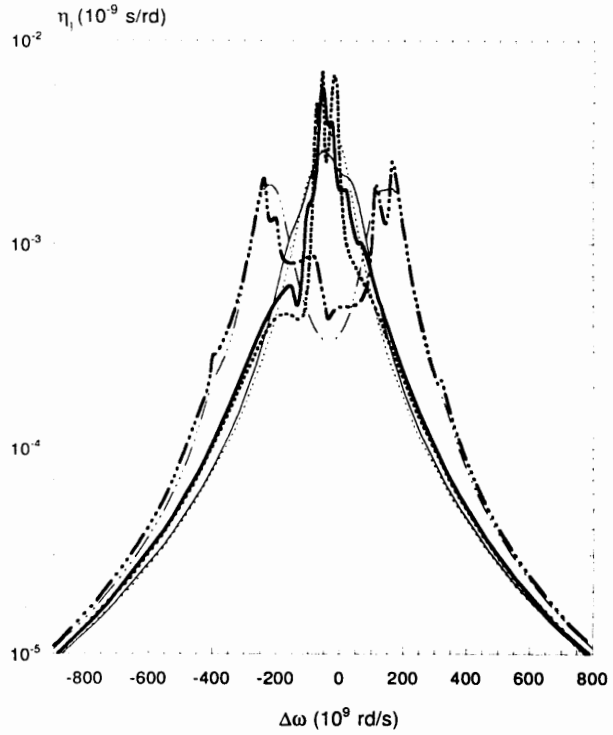

Fig. 15. Ion dynamics effects on η_I for the Lyα line at an electronic density of 10^{15} cm^{-3}, for three values of the magnetic field: 10^3 (dotted lines), 5 10^3 (solid lines), and 2 10^4 G (dots-dashes). Thick lines correspond to profiles computed with the static approximation for the ions, thin lines to profiles taking ion dynamics into account. Fine structure effects are also included.

namics effects. It is calculated without magnetic field or fine structure effects. We shall discuss the consequences of this approximation on the line shapes, calculated including ion dynamics effects, for the three considered values of the magnetic field. At 10^{17} cm^{-3}, the profiles are indistinguishable from the MMM ones and are not shown here. At 10^{15} cm^{-3}, we note a small difference in the line center (less than 5%) (Figures 17, 18). At 10^{13} cm^{-3}, the agreement is still correct when fine structure effects are not taken into account (Figure 20) and we note a larger disagreement between the components when fine structure effects are included (Figure 19). In fact, the first of the two conditions (36) is satisfied only for the lowest magnetic field value. The second condition (36) (i.e., $\omega_{pi} > \omega_{fs}$) is not satisfied at this density. This explains the disagreement in the case where fine structure is included. When the fine structure effects are neglected, the second condition (36) is no longer relevant. The good agreement for all the magnetic field values indicates that the estimate of $\gamma(\omega)$ is reasonably good at this low density.

In the line wings, fine structure, ion dynamics and Zeeman effect vanish in η_I, as shown previously. Fine structure and ion dynamics do not affect η_V. The line shapes obtained in SUT and MMM are identical.

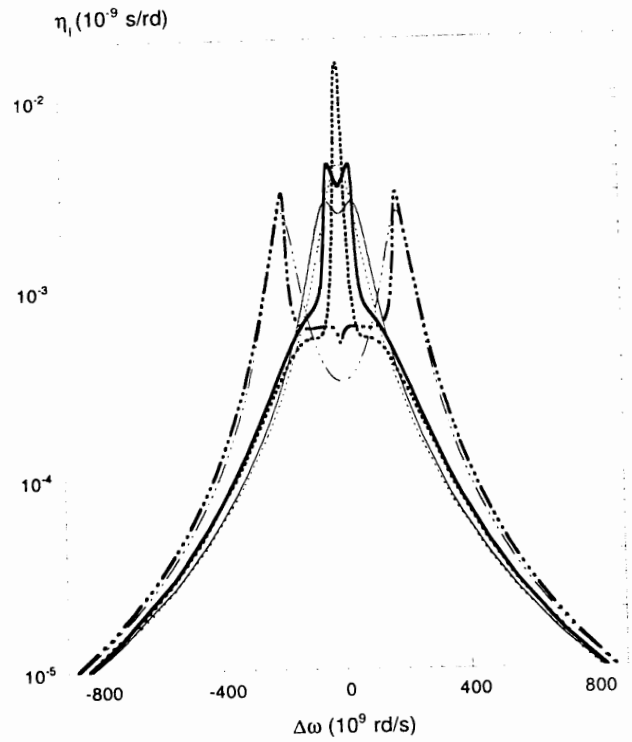

Fig. 16. Ion dynamics effects on η_I for the Lyα line at an electronic density of 10^{15} cm^{-3}, for three values of the magnetic field: 10^3 (dotted lines), 5 10^3 (solid lines), and 2 10^4 G (dots-dashes). Thick lines correspond to profiles computed with the static approximation for the ions, thin lines to profiles taking ion dynamics into account. Fine structure effects are not included.

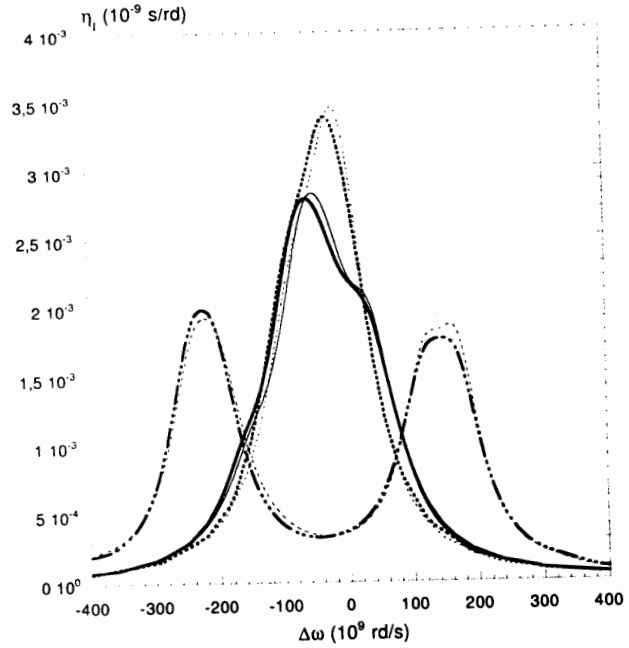

Fig. 17. Comparison between the line shapes (η_I), obtained with the MMM (thin lines), and with the SUT (thick lines), in the center of the Lyα line, at an electronic density of 10^{15} cm^{-3}, for four values of the magnetic field: 10^3 (dotted lines), 5 10^3 (solid lines), and 2 10^4 G (dots-dashes). Fine structure effects are included.

3.5 Relation between η_V and η_I in the line wings

As derived in Sect. 2.4, η_I and η_V should be connected to each other via the longitudinal magnetic field value (which is equal to B for θ equal to zero). In order to check the validity of this result, we introduce the quantity $R(\omega)$ defined by

$$R(\omega) = \frac{\eta_V \, \Delta\omega \, B}{2\eta_I \, \omega_L}, \qquad (40)$$

which has the dimension of a magnetic field.

This quantity is plotted in Figures 21, 22, and 23, for the three electronic densities considered here. The results that are represented have been obtained with the MMM calculation, including or not fine structure effects. As expected $R(\omega)$ converges towards the value of the external magnetic field. The fine structure effects contribute only in the line center.

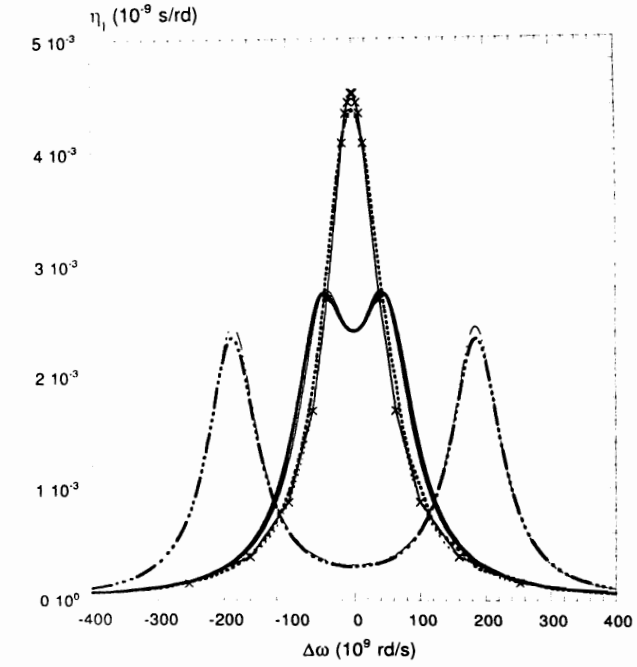

Fig. 18. Comparison between the line shapes (η_I), obtained with the MMM (thin lines), and with the SUT (thick lines), in the center of the Lyα line, at an electronic density of 10^{15} cm^{-3}, for four values of the magnetic field: 0 (crosses), 10^3 (dotted lines), 5 10^3 (solid lines), and 2 10^4 G (dots-dashes). Fine structure effects are not taken into account.

3.6 Discussion

We have analyzed the effects of the fine structure, of the ion dynamics, and of the SUT approximation, in the centre and in the wings of the Lyman α line, for various densities

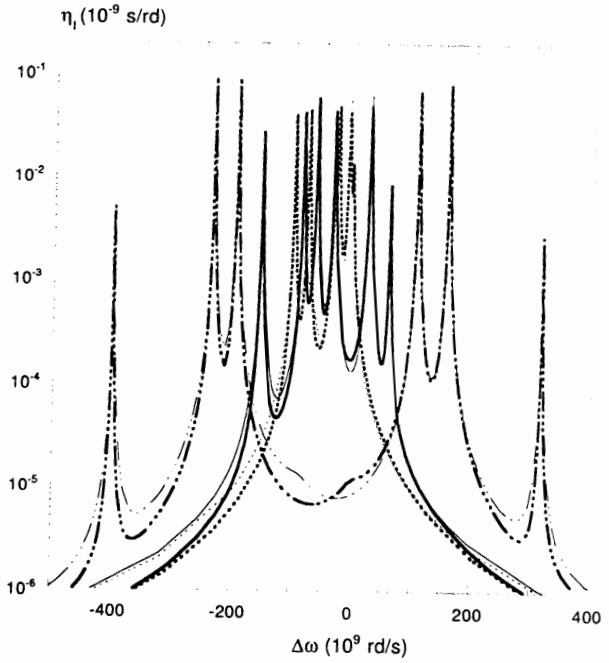

Fig. 19. Comparison between the line shapes (η_I), obtained with the MMM (thin lines), and with the SUT (thick lines), in the center of the Lyα line, at an electronic density of 10^{13} cm^{-3}, for three values of the magnetic field: 10^3 (dotted lines), 5 10^3 (solid lines), and 2 10^4 G (dots-dashes). Fine structure effects are included.

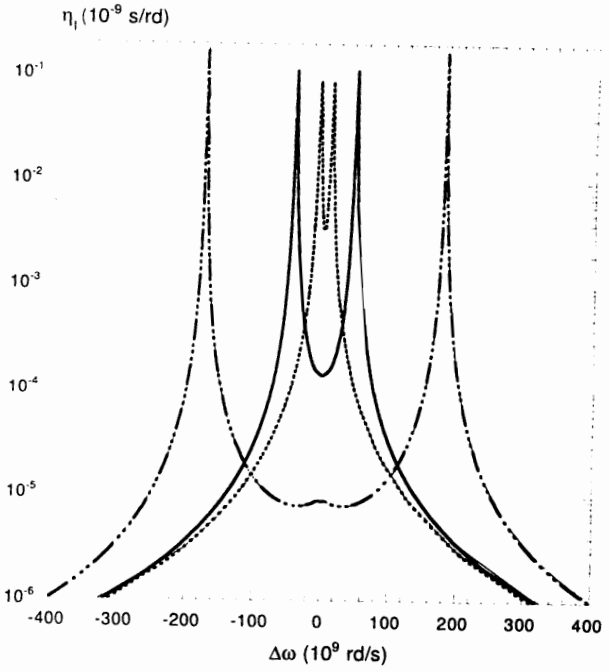

Fig. 20. Comparison between the line shapes (η_I), obtained with the MMM (thin lines), and with the SUT (thick lines), in the center of the Lyα line, at an electronic density of 10^{13} cm^{-3}, for three values of the magnetic field: 10^3 (dotted lines), 5 10^3 (solid lines), and 10^4 G (dots-dashes). At this scale, the MMM and SUT profiles are almost exactly superimposed. Fine structure effects are not taken into account.

and a fixed temperature of 10^4 K. This temperature is representative of the conditions of typical stellar atmospheres and of standard laboratory experiments. Changing it for a given density should not modify the conclusions already given. In particular, the fine structure effects are expected to be significant only in the line centre and at low densities. The SUT and "exact" MMM line shapes converge towards each other in the line wings. They are also close together in the line centers. This is illustrated in Figure 24, which shows on a logarithmic scale and for positive detunings, the profile η_I for an electronic density equal to 10^{14} cm^{-3} (without motional Stark effect), and temperatures equal to 10^4, 10^6, and 10^7 K. We note that the line width decreases with increasing temperature, in agreement with the width variation in $T^{-1/2}$ at low density [32]. However, at the highest temperatures (i.e., greater than 10^7 K), the motional Stark effect can be of the same order of magnitude as the Zeeman effect (see Equations 1,17), and it should also affect the centre of the profiles η_I and η_V.

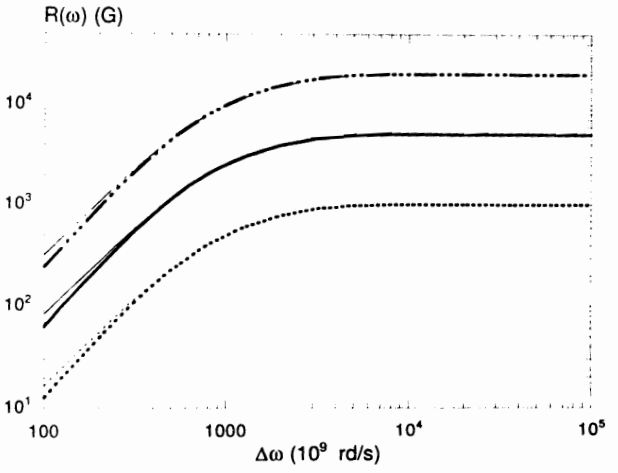

Fig. 21. $R(\omega)$ (Equation (40)) vs. the positive detuning, for an electronic density of 10^{17} cm^{-3} and three values of the magnetic field: 10^3 (dotted lines), 5 10^3 (solid lines), and 2 10^4 G (dots-dashes). The profiles including the fine structure effects are represented as thin lines, those neglecting the fine structure effects as thick lines.

4 Conclusions

We have calculated accurate generalised polarised line shapes of hydrogen Lyα line in a large range of plasma density and magnetic field values. We have inspected the effects of fine structure, and ion dynamics. We have shown that it is essential to include ion dynamics effects, in the line centers. Fine structure also plays a very significant rôle at low

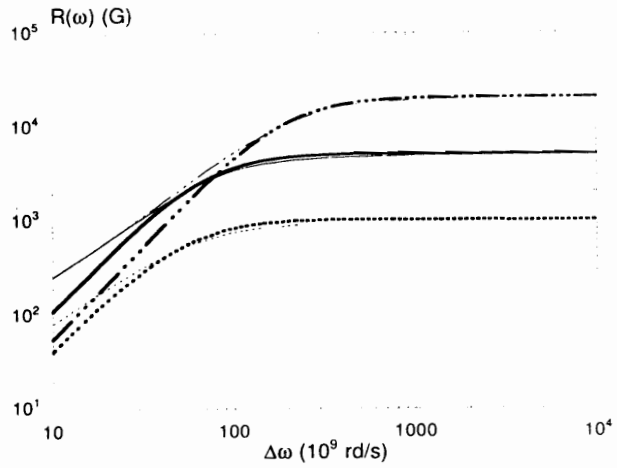

Fig. 22. Same as Figure 21 but for an electronic density of 10^{15} cm^{-3}.

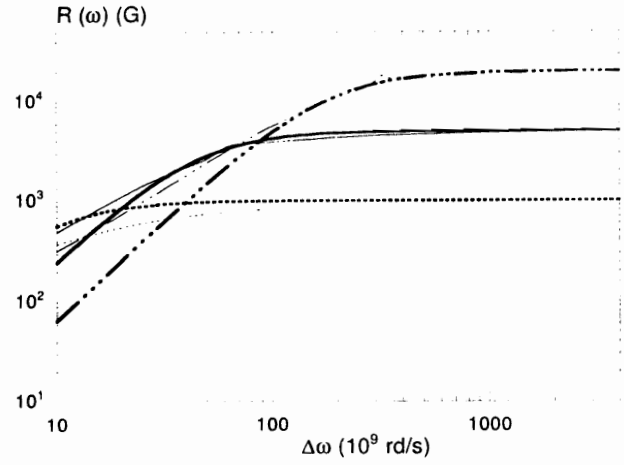

Fig. 23. Same as Figure 21 but for an electronic density of 10^{13} cm^{-3}.

density. In the line wings, however fine structure and ion dynamics can be neglected. The profiles in η_V and η_I, and the value of the longitudinal magnetic field, are connected through a relation (Equation (30)) which differs from the traditional one (Equation (35)). The use of the Simplified Unified Theory is always justified in the line wings, and for $N_e \geq 10^{15}$ cm^{-3} in the line centre. This can be helpful for extensive calculation of more complicated lines, as $H\beta$, due to a huge reduction of the required computer time allowed by this method.

S. Brillant thanks the "Société de Secours des Amis de la Science" for its support during his thesis. Part of this work was done during a stay of G. Mathys as Visiting Professor at the Observatoire de Paris-Meudon (DASGAL), the support of which is gratefully acknowledged.

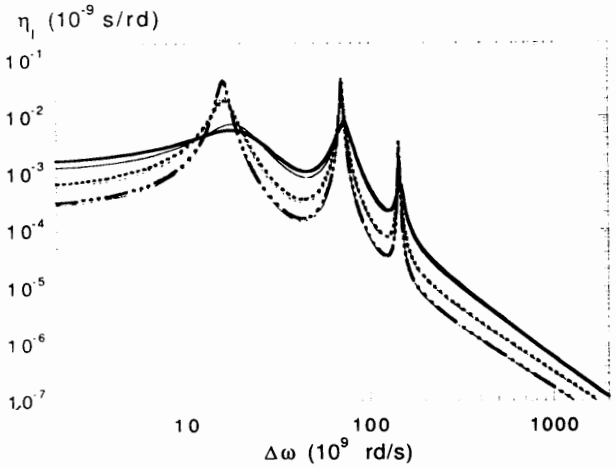

Fig. 24. Comparison between the line shapes (η_I), obtained with the MMM (thin lines) and with the SUT (thick lines), in the centre of the Lyα line, at an electronic density of 10^{14} cm^{-3} and in a magnetic field of 10^4 G, for three values of the temperature: 10^4 (solid lines), 10^6 (dashed lines), and 10^7 K (dots-dashes). Fine structure effects are taken into account.

References

1. Nguyen Hoe, Drawin H.W., Herman, L. J. Quant. Spectrosc. Rad. Transfer **7** (1967), 429.
2. Djurović S., Mijatović Z., Pavlov M., Vujivić B., Kobilarov R., Nikolić D., Publ. Obs. Astron. Belgrade **50** (1995), 65.
3. Demura A., Oks E., IEEE Trans. Plasma Science **26** (1998), 1251.
4. Günter S. , Könies A., J. Quant. Spectrosc. Rad. Transfer **62** (1999), 425.
5. Deutsch C., Phys. Rev. **A2** (1970), 1258.
6. Nguyen Hoe, Grumberg J., Caby M., Leboucher E., Coulaud G., Phys. Rev. **A24** (1981), 438.
7. Mathys G., *Hydrogen line formation in dense plasmas in the presence of a magnetic field*, in *Progress in Spectral Line Formation Theory*, J.E. Beckman, L. Crivellari (eds.) (Reidel, Dordrecht, 1985), 381.
8. Mathys G., J. Quant. Spectrosc. Rad. Transfer **44** (1990), 143.
9. Mathys G., Astron. Astroph. Suppl. Series **59** (1985), 229 .
10. Mathys, G., Astron. Astroph. **139** (1984), 196.
11. Brillant S., Mathys G., Stehlé C., Astron. Astroph. **339** (1998), 286.
12. Brillant S., Thesis, Université de Paris XI (1999).
13. Greene R.L., J. Quant. Spectrosc. Rad. Transfer **27** (1982), 639 .
14. Ruder H., Wunner G., Herold H., Geyer F., *Atoms in Strong Magnetic Fields* (Springer, 1994).
15. Stehlé C., Feautrier N., J. Physique **47** (1986), 1015.
16. Landi Degl'Innocenti E., Landi Degl'Innocenti M., Il Nuovo Cimento **27B** (1975), 134.
17. Bransden B.H., Joachain C.J., *Physics of atoms and Molecules* (Longman Scientific Technical, 1983).
18. Casini R., Landi Degl'Innocenti E., Astron. Astroph. **276** (1993), 289
19. Demkov Yu. N., Monozon B. S., Ostrovskii, Sov. Phys. JETP **30** (1970), 775.

20. Hooper C.F., Phys. Rev. **149** (1966), 77.
21. Hooper C.F., Phys. Rev. **165** (1968), 215 .
22. Brissaud A., Frisch U., J. Quant. Spectrosc. Rad. Transfer **11** (1971), 1767.
23. Frisch U., Brissaud A., J. Quant. Spectrosc. Rad. Transfer **11** (1971), 1756 .
24. Stehlé C., Jacquemot S., Astron &Astroph. **271** (1993), 348.
25. Stehlé C., Astron Astroph. Suppl. Ser. **104** (1994), 509.
26. Smith E.W., Cooper J., Vidal, C.R., Phys. Rev. **185** (1969), 140.
27. Stehlé C., Hutcheon R., Astron Astroph. Suppl. Ser. **140** (1999), 93.
28. Wiese W.L., Smith M.W., Glennon B.M., Atomic Transition Probabilities Vol. 1 – Hydrogen through Neon, NSRDS-NBS 4 (1966).
29. Landstreet J.D., Borra E.F., Angel J.R.P., Illing R.M.E., Astroph. J. **201** (1975), 624.
30. Stehlé C., Phys. Rev. **A34** (1986), 4153.
31. Brissaud A., Goldbach C., Léorat J., Mazure A., Nollez G., J. Phys. B: Atom. molec. Phys. **9** (1976), 1129.
32. Stehlé C., Astron &Astroph. **305** (1996), 677.